Applied Catalysis A, General xxx (xxxx) xxx–xxx

Contents lists available at ScienceDirect

Applied Catalysis A, General

journal homepage: www.elsevier.com/locate/apcata

Improvement of the catalytic activity of Ni/SiO_2-C by the modification of the support and Zn addition: Bio-propylene glycol from glycerol

Martin N. Gatti[a,b], Martín D. Mizrahi[c], Jose M. Ramallo-Lopez[c], Francisco Pompeo[a,b], Gerardo F. Santori[a,b], Nora N. Nichio[a,b,*]

[a] CINDECA, Facultad de Ciencias Exactas, Universidad Nacional de La Plata, CCT La Plata- CONICET, 47 N° 257, 1900 La Plata, Argentina
[b] Facultad de Ingeniería, Universidad Nacional de La Plata, 1 esq 47, 1900 La Plata, Argentina
[c] INIFTA, Facultad de Ciencias Exactas, Universidad Nacional de La Plata, CCT La Plata- CONICET, Diagonal 113 y 64, 1900 La Plata, Argentina

ARTICLE INFO

Keywords:
NiZn catalysts
Functionalization
Bio-propylene glycol
Glycerol

ABSTRACT

In previous studies, we prepared Ni catalysts supported on a silica-carbon composite which is selective for obtaining 1,2-propylene glycol (1,2-PG). In order to improve the activity levels of this catalyst, in the present work we propose to modify the catalyst formulation by means of two strategies: on the one hand, to modify the acidity of the catalyst through the functionalization of the carbon support and, on the other hand, to modify the metallic phase by the addition of Zn from a controlled preparation technique (Surface Organometallic Chemistry on Metals), which allows the selective addition of small amounts of modifier on the metallic particles.

The functionalization of the SC support at 80 °C employing HNO_3 at 60 wt% as oxidizing agent allowed increasing the number of surface acid sites that provide Lewis-type acidity without loss of specific surface area.

The addition of 1.1–1.8 wt% of Zn (which corresponds to catalysts NiZn0.2/SC and NiZn0.32/SC) generates the formation of an active site composed of an α-NiZn alloy responsible for the increase in activity. When the addition of Zn is 2.8 wt% (which corresponds to catalyst NiZn0.5/SC), the generation of a new tetragonal phase of β_1-NiZn would cause the decrease of catalytic activity. These results indicate that the Zn addition has a more significant effect upon the activity and selectivity on the C—O bond cleavage reactions than the effect of the support acidity upon the dehydration activity.

1. Introduction

Biomass represents one of the most abundant sources of renewable resources based on polyfunctional molecules which allow the production of clean, sustainable energies and the manufacturing of chemical products, now petrochemically obtained [1,2].

Glycerol, a by-product of biodiesel production, is a compound of second-generation biomass, of low-cost market value which can be transformed into other chemicals of high-added value [3–5]. Specifically, the catalytic hydrogenolysis of glycerol allows obtaining 1,2-propylene glycol (1,2-PG), widely employed in several industries including polymers, pharmaceuticals, cosmetics, foods, and paints, among others [6–8].

The alternative production of 1,2-PG via glycerol would reduce the costs associated with the manufacturing process and would make possible a renewable, clean route thus avoiding its petrochemical processing [9].

The hydrogenolysis reaction can be carried out in liquid phase at moderate temperatures (200–350 °C) and high pressures (20–80 bar) in order to avoid the vaporization of the feedstock [10].

The most widely accepted reaction mechanism involves a first stage of dehydration of glycerol to acetol (AcOH) as intermediate product and its subsequent hydrogenation for the formation of 1,2-PG [9,11]. It is well known that acid sites catalyze this first stage; therefore, a bifunctional catalyst able to both dehydrate and hydrogenate should be designed [12,13].

Noble metals such as Ru, Pd and Pt have been used as active phases of supported catalysts [1,7]. However, they present the disadvantage of promoting the cleavage of C—C bonds generating such by-products as ethylene glycol (EG), methanol (MeOH) and ethanol (EtOH) [8]. Non-noble metals, like Cu and Ni, have shown better performance due to their greater capacity of C—O bond cleavage, with higher yields towards the formation of 1,2-PG [14].

With respect to the supports, the more acid materials like γ-Al_2O_3 and zeolites of types HY, 13X, HZSM-5 and Hβ were studied by Guo et al. [15] in the preparation of Cu catalysts. The order of activity found

* Corresponding author at: CINDECA, Facultad de Ciencias Exactas, Universidad Nacional de La Plata, CCT La Plata- CONICET, 47 N° 257, 1900 La Plata, Argentina.
E-mail address: nnichio@quimica.unlp.edu.ar (N.N. Nichio).

http://dx.doi.org/10.1016/j.apcata.2017.08.037
Received 5 May 2017; Received in revised form 15 August 2017; Accepted 22 August 2017

was Cu/γ-Al_2O_3 > Cu-Hβ > Cu-HY > Cu-HZSM ~ Cu-13X. These results indicate that γ-Al_2O_3 has the appropriate acidity to catalyze the glycerol dehydration to AcOH and, for that reason, the Cu/γ-Al_2O_3 catalyst is more active. The smaller activity found for the rest of the supports was explained by the generation of acrolein instead of acetol, due to the type of acid site and to a greater number of these sites.

Zhao et al. [16] studied catalysts of Ni supported on different types of zeolites (NaX, NaZSM-5, NaMOR, NaA), SiO_2 and γ-Al_2O_3. The order of activity obtained was Ni/NaX > Ni/γ-Al_2O_3 > Ni/SiO_2 > Ni/NaZSM-5 > Ni/NaMOR > Ni/NaA. The best results were associated with the acid sites present in the NaX support.

Another strategy in catalyst formulation is the preparation of bimetallic phases such as Pt-Fe [17], Ru-Cu [5], Cu-Ni [18], Ni-Ag [19], among others.

Soares et al. [17] synthesized bimetallic catalysts of Pt-Fe/Al_2O_3which were more active than the Pt/Al_2O_3catalyst. The addition of Fe generated the formation of a Pt-Fe alloy which improved conversion from 22% to 33% maintaining a selectivity of ~60% towards 1,2-PG at 2 MPa H_2, 220 °C and 12 h of reaction time.

Salazar et al. [5] studied Ru-Cu/TiO_2 bimetallic catalysts and found that the addition of Cu improves the selectivity to 1,2-PG. The catalyst with a Ru/Cu = 1 ratio showed the best performance with a 50% conversion and a 96% selectivity towards 1,2-PG after 12 h on stream at 200 °C and 2.6 MPa H_2.

Bimetallic catalysts of Cu-Ni supported on γ-Al_2O_3 were synthesized by Pudi et al. [18]. With a Cu/Ni = 1 ratio, a 72% conversion and a selectivity of 93% towards 1,2-PG at 210 °C and 4.5 MPa H_2 were reached. The improvement in the catalyst performance was ascribed to the formation of a bimetallic Cu-Ni phase with smaller particle size, higher acidity and better metallic dispersion than phases Cu and Ni separately.

Chen et al. [19] prepared a series of Ni-Ag catalysts and found that for a Ni/Ag = 6 ratio, the catalyst is more active (78% conversion) and selective towards 1,2-PG (~66%) at 210 °C, 4 MPa and 6 h with a 20 wt % glycerol solution. The result was attributed to the formation of a Ni-Ag alloy which increases the glycerol adsorption capacity and enhances the hydrogenation capacity of Ni.

In previous studies, we prepared Ni catalysts supported on a silica-carbon composite which is selective for obtaining 1,2-PG. In order to improve the activity levels of this catalyst, in the present work we propose to modify the catalyst formulation by means of two strategies: on the one hand, to modify the acidity of the catalyst through the functionalization of the carbon support and on the other hand, to modify the metallic phase by the addition of Zn from a controlled preparation technique (Surface Organometallic Chemistry on Metals), which allows the selective addition of small amounts of modifier on the metallic particles.

The functionalized supports were characterized by BET and by acidity measure techniques such as potentiometric titration and the isopropanol decomposition reaction. The bimetallic catalysts were characterized by TEM, XRD and particularly EXAFS in order to determine the presence of a bimetallic phase.

2. Experimental

2.1. Synthesis of the supports

The silica-carbon composite (SC) employed as support was synthesized according to a procedure described elsewhere. The gelling property of TEOS (SILBOND 40-AKZO Chemicals) was used in an alcoholic medium (Ethanol 96% from Anedra) to include a phenol-formaldehyde liquid resin (RL 43003, ATANOR, Argentina) in its structure. With subsequent curing and pyrolisis in reducing atmosphere, this resin leaves a high amount of residual carbon. TEOS and RL 43003, with a 1:1 mass ratio, were mixed on a magnetic stirrer until obtaining an emulsion, to which ethanol was gradually added. Afterwards, pregellification occurred at room temperature for 24 h, drying at 50 °C for another 24 h and complete polymerization by heating to 180 °C (heating rate 10 °C h^{-1}) for 3 h. Finally, calcination took place in a reducing atmosphere during 3 h on an electrical oven at 1580 °C (at 5 °C min^{-1}). This material was denominated SC [20]. The SC support was functionalized with nitric acid (60 wt%) as oxidizing agent for 2 h at different temperatures (80–100 °C). In this preparation, 50 cm^3 of nitric acid solution were employed every 1 g of SC composite and kept in reflux at 80 °C–100 °C, for 2 h. Then, the solution was filtered and the solid washed several times with distilled water up to pH 7. Finally, the solid was dried at 100 °C for 24 h. The functionalized supports were denoted as SCA, where "A" indicates the treatment temperature.

2.2. Synthesis of the catalysts

The catalysts were prepared by incipient wetness impregnation of Ni ($NiCl_2{\cdot}6H_2O$ from Sigma-Aldrich) on supports. Ethanol was used as solvent. The $NiCl_2{\cdot}6H_2O$ concentration in ethanol was calculated so as to obtain 5 wt% of Ni in the final solid. Then, the solid obtained was dried at 120 °C during 12 h and activated in H_2 (50 cm^3 min^{-1}) at 400 °C for 90 min (10 °C min^{-1}).

The bimetallic samples were prepared by the surface organometallic chemistry on metals route (SOMC/M) [21]. Zinc modified systems were prepared by reaction between the Ni/SC catalyst (pre-reduced) and a solution of $Zn(C_2H_5)_2$ in *n*-heptane at 80 °C under flowing H_2. The solids obtained after this procedure could still have some ehtyl groups grafted to the surface. Then, they were washed several times with *n*-heptane at room temperature and dried in flowing Ar (50 cm^3 min^{-1}) at 100 °C for 2 h. The bimetallic catalysts (NiZn) were finally obtained by activation in flowing H_2 (50 cm^3 min^{-1}) at 400 °C. The contents of zinc were in the range 0.08–0.5, expressed as Zn/Ni atomic ratio. The catalysts were denoted as NiZnB/SC, where "B" indicates the Zn/Ni atomic ratio.

2.3. Characterization

The Ni content of samples was determined by atomic absorption spectrometry (Spectrophotometer AA-6650 Shimadzu).The equipment utilized was an IL Model 457 spectrophotometer, with a single channel and double beam.

Adsorption-desorption measurements were performed for a textural characterization. Surface area measurements, the Brunauer–Emmett–Teller (BET) multipoint method and textural analysis were obtained using a Micromeritics ASAP 2020 equipment. The samples were pretreated under vacuum in two 1 h stages at 100 and 300 °C.

XRD patterns were recorded on a Philips 3020 powder diffractometer, using Cu Kα radiation (λ = 1.5418 Å, intensity = 40 mA, and voltage = 35 kV). The patterns were recorded in the range of 2θ = 5°–80°. The crystallite sizes of metallic nickel in the reduced samples were calculated using Scherreŕs equation:

$$d^{XRD} = \frac{K.\lambda}{\beta.\cos(\theta)}$$

where K was taken as 0.89 and β *is* the full width of the diffraction line at half of the maximum intensity in radians (Nickel (111) planes).

The acid base properties of supports were determined by the test of isopropanol decomposition (IPA). This reaction was tested in a continuous-flow fixed-bed reactor between 200 and 300 °C, atmospheric pressure, feed 4.5% IPA in Helium, with a flow of 40 cm^3 min^{-1}.

Potentiometric titrations were performed with 0.05 g of support suspended in acetonitrile (Merck) and stirred for 3 h. Then, the suspension was titrated with 0.05 mol L^{-1} *n*-butylamine (Carlo Erba) in acetonitrile using a Metrohm 794 Basic Titrino apparatus with a double junction electrode.

Transmission-electron microscopy (TEM) images were taken by means of a TEM JEOL 100C instrument, operated at 200 KV. A graphite

pattern was used for calibration. In this analysis, a suspension in 2-propanol was prepared by stirring the solid sample with ultrasound for 10 min.

To estimate the average diameter volume/area (d_{va}), the particles were considered spherical, and it was calculated using the following expression:

$$d_{va} = \frac{\sum n_i \cdot d_i^3}{\sum n_i \cdot d_i^2}$$

where n_i is the number of particles with diameter d_i. Histograms of particle size distribution arose from the analysis of the micro-photographs obtained using the technique of bright field image.

X-ray Absorption (XAS) spectra were acquired at the Ni-K edge (8333 eV) and Zn-K edge (9659 eV) [22], using the XAFS2 beamline of the LNLS (Laboratorio Nacional do Luz Síncrotron, Campinas, Brazil). A Si (111) crystal was employed as monochromator for absorption measurements at the Ni and Zn-K edges; harmonic beam components were less than 1% using this monochromator. All experiments were performed in transmission mode, and beam intensities were measured using a series of three ionization chambers filled with the appropriate gas mixture at ambient temperature and pressure. The photon energies were calibrated by measuring the beam transmission, simultaneously with the sample, through a thin film of metallic foil (Ni or Zn) placed between the second and third ionization chambers. XAS spectra of bimetallic samples were collected at the absorption edges of both metals in a range of 200 eV before and 1000 eV after the corresponding edge. The samples were then transferred under Ar at atmospheric pressure and ambient temperature to an XAS cell hermetically sealed with Kapton® windows. XAS spectra were collected at ambient temperature.

Extended X-ray Absorption Fine Structure (EXAFS) data analyses were carried out using the IFFEFIT package (Athena, Artemis) [23]. Background subtraction and edge-step normalization of the spectra were performed using the *AUTOBK* algorithm implemented in Athena. Structural information for the metals, including coordination numbers (*N*), interatomic distances (R), and their Debye-Waller factors (σ^2), were obtained from Artemis using nonlinear least squares fits of the Fourier transformed data in r-space, with theoretical amplitudes and phase shifts for all single scattering paths calculated by FEFF [24]. All data fits were conducted between 1.0–3.0 Å in r-space and were generated by Fourier filtering the k^3-weighted EXAFS over 2–13 $Å^{-1}$ in k-space with a Hanning window. The theoretical scattering path amplitudes and phase shifts used in these fits were calculated from crystallographic structures of either monometallic lattices (for Ni-Ni [ICSD number: 64989] and Zn-Zn [ICSD number: 64990] paths) or mixed phase lattices (for Ni-Zn and Zn-Ni [25] paths), all of which were face-centered cubic (*fcc*). EXAFS data extracted from bimetallic samples were fit simultaneously at both metal edges, thus ensuring consistency in the interatomic distances and Debye-Waller factors of bimetallic paths. Photoelectron single scattering by low-Z species (O), with theoretical amplitudes and phases calculated from metal oxide (NiO [ISCD number: 9866] and ZnO [ISCD number: 67454]) crystal structures, was also included in the fits to examine the contribution of these non-metallic bonds to the EXAFS. Passive reduction factors (S_0^2) [22] for each metal (Ni: 0.8 and Zn: 0.78) were obtained from single scattering fits to the EXAFS spectra of the metal foils by constraining the coordination number to 12 in each case.

2.4. Catalytic activity test

Glycerol hydrogenolysis reactions were carried out in a stainless steel high pressure reactor BR-100 system, from Berghof Instruments, with a volume of 100 mL, operated in batch mode.

The catalyst was reduced ex situ at 400 °C for 90 min in H_2 flow (30 $cm^3 min^{-1}$) using a heating rate of 10 °C min^{-1}. The catalysts were cooled down to room temperature under hydrogen stream and immediately transferred to the reactor containing the glycerol aqueous solution. Then, the reactor was closed, purged and pressurized with pure H_2 or N_2 (Air Liquide, 99.99%) at 2 MPa. Afterwards, heating was started (6 °C min^{-1}) and when the reactor was at 260 °C, autogenous pressure reached a value of 5.5 MPa and stirring began. The magnetic stirring was set at 1000 rpm to ensure kinetically controlled conditions.

After reaction, the system was cooled to ambient temperature and liquid and gaseous samples were collected. For the analysis and quantification of gaseous products, a Shimadzu GC-8A chromatograph equipped with a thermal conductivity detector (TCD) with a Hayesep D 100-120 column was used. For the analysis and quantification of liquid products a GCMS-QP505A Shimadzu chromatograph was used, equipped with a 19091S-001 HP PONA, 50 m capillary column and with FID and MS detectors.

The accuracy of the measured values was within 5%, and the experiments could be reproduced with a relative error of 10%. Carbon balance for all runs was close to within 98%.

The total conversion of glycerol (X_T) was determined as follows:

$$X_T(\%) = \frac{moles\ \ of\ \ consumed\ \ glycerol}{moles\ \ of\ \ initial\ \ glycerol}.100$$

The conversion of glycerol to liquid products (X_L) was determined as follows:

$$X_L(\%) = \frac{\sum\ moles\ \ of\ \ carbon\ \ in\ \ liquid\ \ products}{moles\ \ of\ \ carbon\ \ in\ \ initial\ \ glycerol}.100$$

The selectivity of liquid products were defined as:

$$Selectivity\ \ of\ \ liquid\ \ products\ (\%) = \frac{moles\ \ of\ \ carbon\ \ in\ \ specific\ \ product}{\sum\ moles\ \ of\ \ carbon\ \ in\ \ liquid\ \ products}.100$$

3. Results and discussion

3.1. Support characterization

The isotherms obtained by N_2 adsorption-desorption of SC and functionalized SC composites are type IV isotherms with H3 hysteresis loops according to the IUPAC classification available in the supplementary information (S1a) [26]. BET specific surface area values, total pore volume and pore characteristics are shown in Table 1. The presence of mesopores was observed in all materials. Micropore surface (S_{micro}) and micropore volume (V_{micro}) were estimated using the t-plot method, while the mesopore surface (S_{meso}) was calculated by subtracting S_{micro} from S_{BET} [27].

Table 1
Physical-chemical and textural properties of Ni/SC, Ni/SC80, NiZn0.2/SC and NiZn0.5/SC reduced catalysts and textural properties of SC supports.

Sample	BET						TEM	
	S_{BET}[a]	V_p[b]	Micropores		Mesopores		d_{av} (nm)	D (%)
			S_{micro}[c]	V_{micro}[d]	S_{meso}[e]	V_{meso}[f]		
SC	208	0.28	54	0.02	154	0.26	–	–
SC80	290	0.51	90	0.03	200	0.48	–	–
SC90	245	0.42	70	0.03	175	0.39	–	–
SC100	176	0.30	33	0.01	143	0.29	–	–
Ni/SC	202	0.48	52	0.02	150	0.46	8.5	11.1
Ni/SC80	262	0.41	89	0.04	173	0.37	9.2	10.5
NiZn0.2/SC	190	0.37	53	0.02	137	0.35	10.7	9.1
NiZn0.5/SC	156	0.31	44	0.02	112	0.29	13.4	7.2

[a] Specific surface area ($m^2 g^{-1}$).
[b]Total pore volume ($cm^3 g^{-1}$).
[c,d]Specific surface area ($m^2 g^{-1}$) and total pore volume for micropores ($cm^3 g^{-1}$).
[e,f]Specific surface area ($m^2 g^{-1}$)and total pore volume for mesopores ($cm^3 g^{-1}$).
$D\% = \frac{97}{d_{va}} \times 100$.

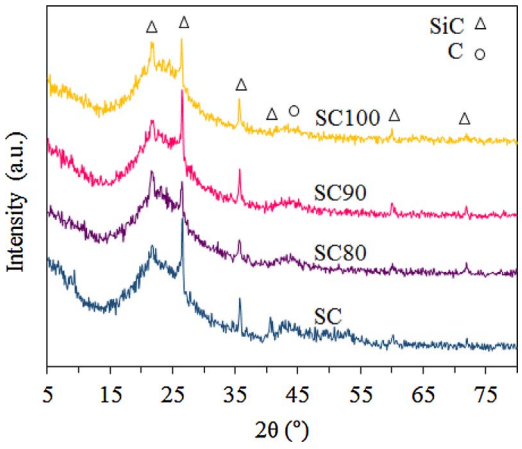

Fig. 1. XRD patterns of SC and SC functionalized.

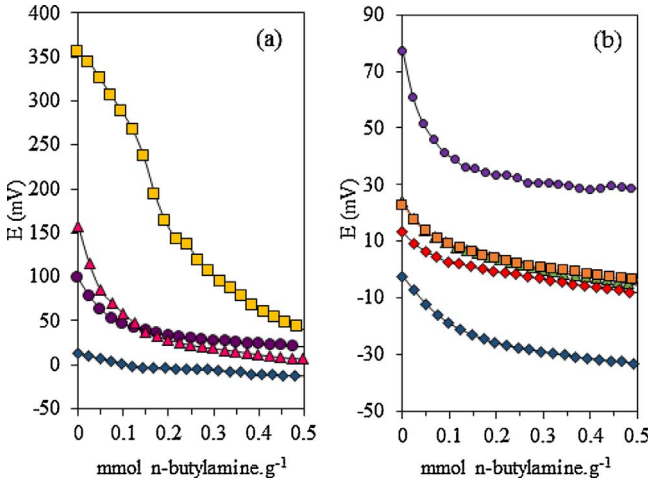

Fig. 2. Potentiometric titration curves with *n*-butylamine in acetonitrile of (a) SC (♦), SC80 (●), SC90 (▲) and SC100 (■) (b) Ni/SC (♦), Ni/SC80 (●), NiZn0.2/SC (▲), NiZn0.32/SC (■) and NiZn0.5/SC (♦).

The functionalization treatments performed at 80 °C and 90 °C produced an increase in the BET surface area. This increase, together with the increase in total pore volume, has already been explained in the literature by the partial gasification of carbon provoked in the oxidation process [28]. When the functionalization treatment was performed at 100 °C, a decrease was observed in the BET surface area, which could be due to the growth of oxygenated groups that provoked wall destruction and pore collapse [29].

Fig. 1 shows the X-ray diffractograms for SC and functionalized composites. The presence of a broad band between 2θ = 15 and 30° is observed, characteristic of the silica amorphous band [30,31]; as well as the peaks at 2θ = 21.8°, 26.4°, 35.7°, 41.4°, 60.0° and 71.9° assigned to the (0 0 4 8), (0 1 1), (1 1 1), (2 0 0), (2 2 0) and (3 1 1) planes of silicon carbide (Δ) (JCP 29-118, JCPDS 29-129) [32,33].

A signal at 2θ = 43.7° assigned to the (1 0 0) plane of the hexagonal phase of graphitic carbon (○) [31,34] can be observed. The peaks corresponding to the graphitic carbon hexagonal phase (1 0 2), (0 0 4) and (1 0 3) at 2θ = 51°, 54.5°, 59° respectively cannot be distinguished. This could be due to the formation of turbostratic carbon. The presence of turbostratic carbon produces a shift of the peaks to lower angular values of 2θ and, in this case, they could overlap the silica amorphous band [35]. In Fig. 1, it can be observed that the functionalized samples present not differences and that the treatments in HNO_3 do not alter the structure of the SC composite.

By means of potentiometric titration with *n*-butylamine, it is possible to estimate the strength and the number of acid sites present in a solid. It is considered that the initial potential (E_i) indicates the maximum strength of the acid sites present in a solid. The acidic strength of surface sites can be assigned according to the following ranges: very strong site, Ei > 100 mV; strong site, 0 < Ei < 100 mV; weak site, −100 < Ei < 0 mV and very weak site, Ei ≤ 100 mV. If the titration curve changes the concavity, it is considered that the point of inflection indicates the presence of more than one type of acid site [36,37].

Fig. 2a shows the potentiometric titration curves for SC supports; an increase in acidic strength with the increase of the functionalization temperature can also be observed. The shapes of the curves for samples SC80 and SC90 indicate that there is only one type of acid sites whereas the curve for SC100 indicates that there are two types of sites.

The nature of acid sites generated by the HNO_3 treatment was determined according to Boehm's method and is available in the supplementary information (S2). SC and SC80 supports present the highest concentration of carboxyl groups, among the surface groups titrated. Functionalization of SC generates an increase in lactonic and carboxyl groups, which gives an increase in their Lewis activity to the SC80 [20].

The results of the isopropanol decomposition reaction (IPA) employing these supports (Table 2) show that the most active sample is SC80. This reaction has been reported as an indirect measure to characterize acidity, basicity and strength of sites. They are classified according to their capacity to dehydrate or dehydrogenate, leading to the formation of propylene, diisopropyl ether (DIPE) and water by dehydration, or the formation of acetone and hydrogen by dehydrogenation. When propylene and DIPE are produced, surface sites are strong Lewis acid and base sites. When propylene and acetone are produced, weak Lewis acid sites or strong base sites can be found. If the only reaction product is propylene, the sites can be either strong Lewis or Brønsted acids [38].

Table 2
Selectivity to propylene ($S_{propylene}$) and acetone ($S_{acetone}$) in isopropanol decomposition reaction.

Support	Isopropanol decomposition X_{IPA} = 14%		
	T (°C)	$S_{propylene}$ (%)	$S_{acetone}$ (%)
SC	360	76	24
SC80	330	93	7
SC90	340	93	7
SC100	360	98	2

Reaction conditions: 4.5% IPA in Helium 40 cm^3 min^{-1}.
X_{IPA}: IPA conversion.

The results shown in Table 2, for an IPA conversion of 14%, indicate that the products are mainly propylene and, to a lesser extent, acetone. This would indicate that these materials have a low contribution of basic sites. The increase of the selectivity to propylene in functionalized materials would indicate an increase of Lewis or BrØnsted acid sites. The higher acidity and the greater BET surface area of SC80 provoke the greater activity in IPA decomposition reaction.

3.2. Catalyst characterization results

Table 1 shows the characterization results of catalysts Ni/SC, Ni/SC80 and bimetallic NiZn/SC, after being reduced in hydrogen flow at 400 °C for 90 min.

The results of adsorption by the BET method show that the addition of Ni does not affect the surface area; while the NiZn0.5/SC catalyst, with the highest Zn addition, has a smaller S_{BET}. The isotherms are available in the supplementary information (S1b).

Table 1 indicates the average diameter d_{va} and the metallic dispersion determined by TEM for the catalysts. Ni/SC and Ni/SC80 present values of the average diameter d_{va} of 8.5 nm and 9.2 nm that would correspond to very similar metallic dispersions of 11 and 10.5% respectively. The TEM images have been included in the S3

supplementary information. Unlike our results, Zhang et al. [39] observed an increase in the metallic dispersion due to the generation of surface oxygenated groups. These authors treated the coconut shell activated carbon (S_{BET} = 1640 m^2 g^{-1}) with nitric acid 4 M.

The bimetallic NiZn0.2/SC catalyst has a slightly longer d_{va} than the Ni/SC catalyst. As the Zn/Ni of 0.2–0.5 ratio increases, the average diameter increases from 10.7 to 13.4 nm. This result is in agreement with what was reported by Melo et al. [40], who observed an increase in particle diameter of 10 nm to 17 nm with an increase in the content of Zn in catalysts NiZn/SiO_2.

Fig. 2b presents the potentiometric titration curves for catalysts Ni/SC, Ni/SC80 and NiZn/SC. If these curves are compared with those obtained for the supports (Fig. 2a), it can be observed that the addition of Ni reduces the surface acidity, most probably due to the interaction of the metallic precursor with those sites. It can also be observed that the increase in acidic strength for the functionalization treatment is greater than the increase due to the presence of Zn in bimetallic catalysts. Moreover, the NiZn0.5/SC catalyst shows a slight decrease in the Ei value with respect to catalyst NiZn0.2/SC.

The XRD results show no differences in the diffractograms of Ni/SC and Ni/SC80 (data not shown). Fig. 3 shows the XRD diffractograms of Ni/SC and NiZn/SC reduced catalysts. The little peak at 2θ = 35.58° present in all samples is due to the SC support (Fig. 1). For the Ni/SC catalysts, the principal peaks of metallic Ni are observed (2θ = 44.4° and 51.7°), with a lattice parameter a = 3.525 Å. The average crystallite size estimated using the Scherrer relation is close to 8.8 nm, in agreement with the TEM measurement. For the NiZn/SC catalysts, the XRD results indicate neither the presence of metallic Zn nor the presence of metallic Zn or segregated ZnO. The Ni characteristic peaks become wider and shift to smaller angles with increasing Zn loading (see inset in Fig. 3). According to the literature [41], this shift suggests Ni-Zn solid solution formation. The main peak was fitted using two Voigt functions (Peak 1 and 2) as shown in Table 3 and Fig. 4. Each component of the fit can be associated with the formation of a α-NiZn alloy with different Zn content. From the variation of the lattice parameters obtained, and using the linear relation reported by Pearson and Thompson [41], the Zn percentage present in each alloy can be estimated (see Fig. S4 and Table 3). For sample NiZn0.08/SC, peak 1 has a content of 12.7% of Zn, while peak 2 has a 2.2% of Zn. For sample NiZn0.5/SC, the Zn content increases to 23% in peak 2. Besides, in sample NiZn0.5/SC there appears a new peak at 2θ = 46.7°, which demonstrates the formation of a new crystallographic phase that coexists with those previously mentioned. According to Friedrich et al. [42], the new phase formed corresponds to tetragonal β_1-NiZn. The assignment of the β_1-NiZn phase was performed starting from a diffractogram of sample NiZn0.5/SC in a range of 2θ = 40–80°. This figure is shown in the Supplementary Information (S5). In this new

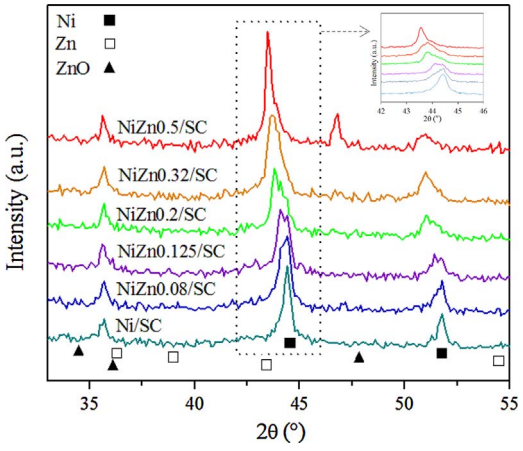

Fig. 3. XRD patterns of Ni/SC and NiZn/SC reduced catalysts.

Table 3
Fitted peaks positions, calculated lattice parameter and estimated Zn concentration for each α-NiZn phase (Peaks 1 and 2).

Sample	Peak 1 position (°)	Lattice parameter (a_1) (Å)	NN distance (Å)	% Zn
NiZn0.08/SC	44.16	3.547	2.508	12.7
NiZn0.125/SC.	44.13	3.553	2.512	15.6
NiZn0.2/SC	43.85	3.580	2.531	27.1
NiZn0.32/SC	43.72	3.583	2.534	28.4

Sample	Peak 2 position (°)	Lattice parameter (a_2) (Å)	NN distance (Å)	% Zn
NiZn0.08/SC	44.43	3.522	2.490	2.2
NiZn0.125/SC	44.42	3.527	2.494	4.3
NiZn0.2/SC	44.08	3.554	2.513	15.7
NiZn0.32/SC	44.02	3.558	2.516	18.0
NiZn0.5/SC	43.85	3.572	2.526	23.4

figure, (S5), it is possible to observe the presence of other peaks that confirm the presence of the β_1-NiZn phase.

Fig. 5a and b shows the extracted EXAFS oscillations at the Ni and Zn K edges, respectively, for every sample. The oscillations of the metals are shown for comparison purposes. EXAFS oscillations at the Ni K-edge of all samples are almost identical to those of the Ni foil. However, the oscillations at the Zn K-edge show a very different behavior and they do not correspond to those of the Zn foil. These characteristics observed at both edges indicate that the Zn atoms are being incorporated into the crystalline structure of Ni.

Vassilev et al. [43] reported that the Zn solubility on Ni is about 30 at.%. For this reason, for the samples with lower Zn/Ni atomic relations, the paths for the first coordination shell of the absorbing atom in the bimetallic structures (Ni-Zn and Zn-Ni) were calculated from the Ni *fcc* structure filled with Zn atoms at random positions in proportion with the Zn/Ni atomic ratio of each sample. For sample NiZn0.5/SC, the β_1 phase of the NiZn alloy was used [25].

Fig. 5c and d shows the Fourier transforms of the EXAFS oscillations and the corresponding fits obtained for each sample at both edges. The obtained parameters are shown in Table 4a and b. No contribution of a metallic Zinc structure is found in any sample, and it can also be observed that part of the Zn atoms is oxidized as a Zn-O shell is fitted, but no Ni-O shell is found in any sample. For this reason, the main analysis will be made from the fits obtained for the data at the Ni K-edge.

For all samples with Zn/Ni ≤ 0.32 the results at both edges are consistent with the formation of a solid solution of Zn in the Ni *fcc* structure. In addition, an increase of the Ni-Zn coordination number is observed as the Zn/Ni ratio is higher, showing that more Zn atoms are incorporated into the Ni fcc structure. Nevertheless, the total coordination number for Ni atoms remains constant for Zn/Ni ≤ 0.32, which is indicating that the surface area to volume ratio for the Ni particles remains almost constant for these Zn contents.

The NiZn0.5/SC sample has a smaller total coordination number, which could be the result of the presence of smaller particles; however, there is no evidence of this in the XRD or TEM results. Given the fact that in sample NiZn0.5/SC there is no other Ni phase besides that of α-NiZn and β_1-NiZn, the decrease in the coordination number could be due to the deformation of the particles upon the support, which would increase the surface/volume ratio, and would produce a decrease in the coordination number observed [44].

Results at the Zn K-edge follow the same trend, indicating that by increasing the Zn content, there appears a Zn-Zn shell with distances similar to those of the Zn-Ni shell, suggesting that they are produced by a higher amount of Zn atoms in the Ni-Zn solid solution and not from a metallic Zn structure. A Zn-O shell fitted is indicating that a fraction of Zn atoms is oxidized, but as no ZnO peaks are observed in the diffractograms, this oxide could be located on the surface of the bimetallic

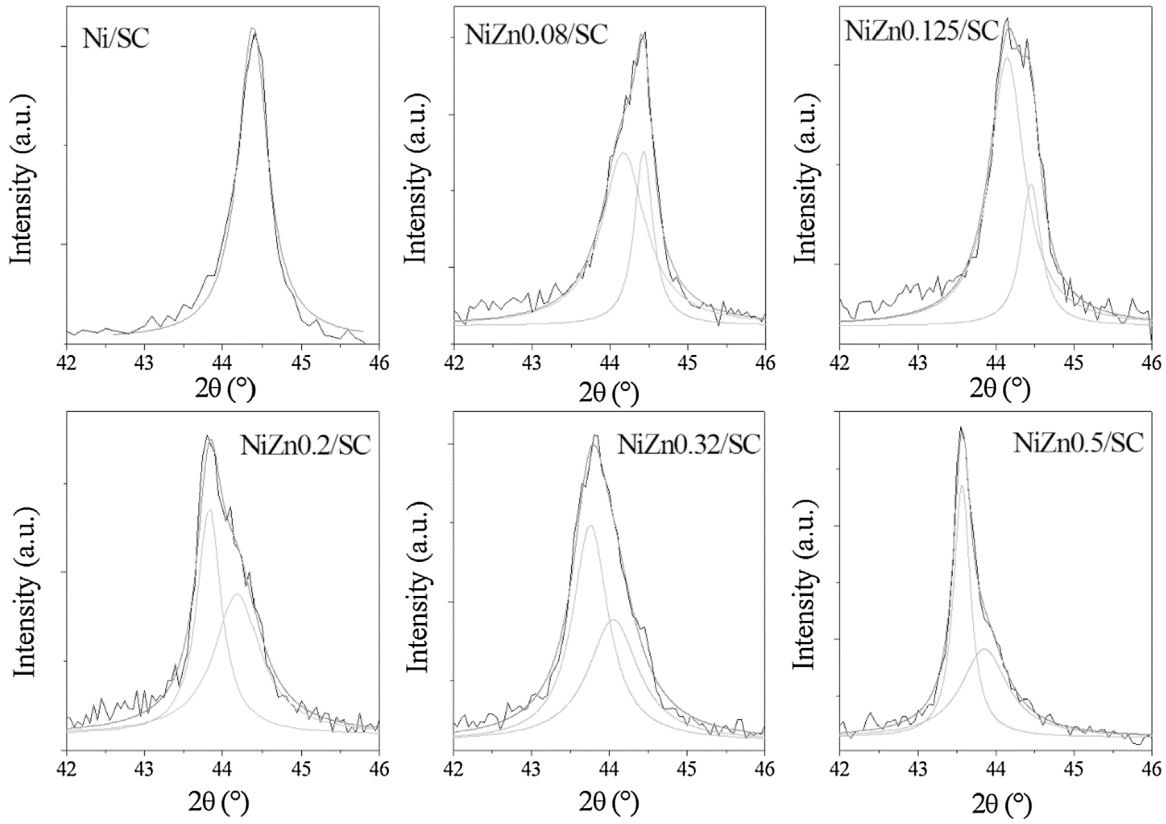

Fig. 4. Fitted main peak for Ni/SC and NiZn/SC samples using Voigt functions.

particles.

3.3. Catalyst activity results

The aim of this work is to study the catalytic activity in the glycerol hydrogenolysis reaction to obtain 1,2-PG. The most widely accepted mechanism of this reaction in acid medium involves a first stage of glycerol dehydration to acetol as intermediate product, and a second stage of hydrogenation for the formation of 1,2-PG [9,11]. For this reason, the study of the catalytic activity of the glycerol hydrogenolysis reaction (*Test (i)*) was complemented with two additional tests: *Test (ii)* the reaction of dehydration and/or C—O bond cleavage of glycerol; and *Test (iii)* the hydrogenation reaction of acetol.

The results of the catalytic activity in the hydrogenolysis reaction of glycerol in liquid phase at 260 °C and 2 MPa of hydrogen pressure (*Test (i)*) are shown in Table 5.

The difference between the total conversion (X_T) and the conversion to liquid products (X_L), would indicate the conversion to gaseous products. In Table 5 it can be observed that for all the catalysts the production to gases is very low.

The reaction products in liquid phase that were identified and quantified were the following: from C1: methanol (MeOH), from C2: ethanol (EtOH), ethylene glycol (EG), from C3: acetone (AcO), 1-propanol (1-POH), acetol (AcOH) and 1,2-propylene glycol (1,2-PG). Table 5 shows that all catalysts were highly selective towards 1,2-PG (> 78%).

If the effect of the support functionalization on the catalytic activity is analyzed, it can be observed that conversion increases for the modified supports. The best result was obtained with Ni/SC80, which reached a conversion of 49% with a selectivity towards 1,2- PG ~85% for 2 h on reaction. This level of selectivity towards 1,2-PG is quite remarkable if compared to what has been reported in the literature. Chen et al. [19] evaluated the activity of a commercial catalyst of Ni Raney (64 wt% of Ni) and obtained a glycerol conversion of 66% with a selectivity towards 1,2-PG of 48% (20 wt% of glycerol, 4 MPa of H_2, 210 °C and 6 h). Dasari et al. [10] evaluated commercial catalysts of Ni/C and Ni/silica-alumina obtaining conversions of 40–45% and selectivities of 68–64%, respectively (80% of glycerol, 1.4 MPa of H_2, 200 °C and 24 h). Xia et al. [45] reported a catalyst of Ni/ZnO with 17 wt% of Ni with a metallic dispersion of 10% and obtained 57% conversion with a selectivity towards 1,2-PG of 44% (500 mg of catalyst, 235 °C, 3 MPa of N_2, 6 h).

In the dehydration reaction of glycerol to AcOH in nitrogen atmosphere (*Test (ii)*), results confirmed that Ni/SC80 is more active than Ni/SC due to the higher acidity of the catalyst shown by the characterization results. With respect to the hydrogenating activity (*Test (iii)*: acetol hydrogenation), it can be observed that catalysts Ni/SC and Ni/SC80 have a similar conversion level most probably due to their similarity in metallic dispersion.

If the effect of Zn addition to catalyst Ni/SC is analyzed, it can be observed that conversion and selectivity towards 1,2-PG are always higher than those obtained with the monometallic catalysts (Ni/SC and Ni/SC80). Table 5 shows that catalysts NiZn0.2/SC and NiZn0.32/SC reach maximum values of conversion (56–57%) and selectivity towards 1,2-PG (86–87%).

Li et al. [46] evaluated catalysts of ZnNiAl hydrotalcite and found that the addition of Zn strongly affects activity and selectivity due to the greater oxophilicity of Zn which facilitates the cleavage of the C—O bonds of glycerol.

The simultaneous increase of conversion and selectivity, shown in Table 5, is indicating the formation of an active site of different nature from that of the original Ni/SC catalyst. In fact, the characterization results showed that the addition of Zn up to 1.8 wt% (NiZn0.32/SC) generates the formation of a α-NiZn alloy which could be the phase responsible for the increase in activity. When the addition of Zn is of 2.8 wt% (NiZn0.5/SC), the generation of a new tetragonal phase of β_1-NiZn could cause the decrease in catalytic activity.

Test (ii) favors the dehydration reaction and the reactions of the

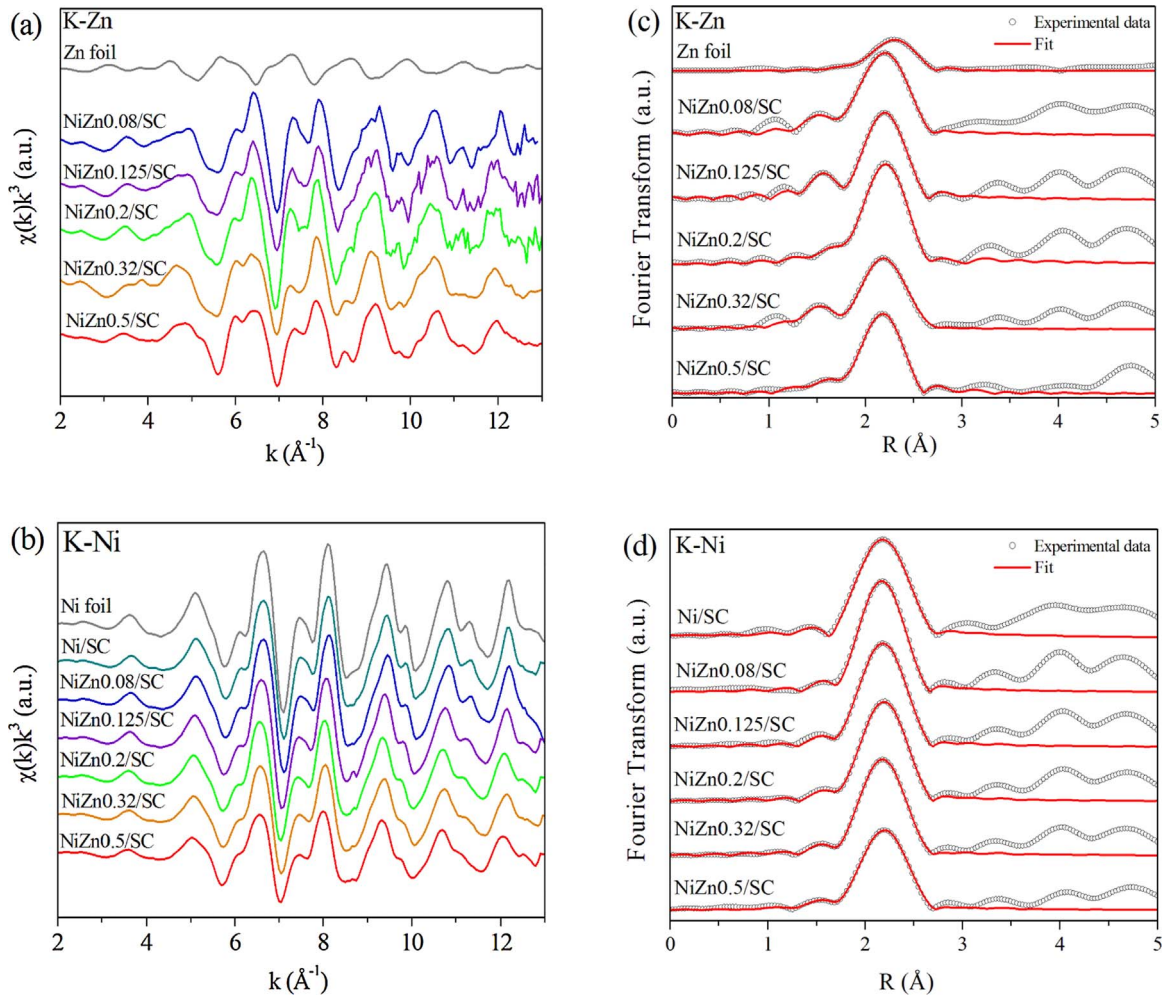

Fig. 5. Extracted EXAFS oscillations at the Zn (a) and Ni (b) k edges for every sample and Fourier transforms of the EXAFS oscillations and the corresponding fits obtained for each sample at Zn K-edge (c) and Ni K-edge (d).

Table 4
(a) Fitted structural parameters obtained from the EXAFS data at the Zn K-edge (b) Fitted structural parameters obtained from the EXAFS data at the Ni K-edge.

(a)

Sample	N_{Zn-O}	R_{Zn-O}	σ^2_{Zn-O}	N_{Zn-Zn}	R_{Zn-Zn}	σ^2_{Zn-Zn}	N_{Zn-Ni}	R_{Zn-Ni}	σ^2_{Zn-Ni}
Zn foil	–	–	–	12*	2.743(4)	0.0090(6)	–	–	–
ZnO	4*	1.973(4)	0.003(1)	–	–	–	–	–	–
NiZn0.08/SC.	1.8(4)	1.965(8)	0.007(1)	–	–	–	7.7(8)	2.51(1)	0.0062(5)
NiZn0.125/SC	1.5(5)	1.945(7)	0.005(1)	–	–	–	7.4(9)	2.51(1)	0.0066(8)
NiZn0.2/SC	0.9(4)	2.03(1)	0.006(1)	1.1*	2.52(1)	0.0076(7)	8.9(9)	2.53(1)	0.0070(8)
NiZn0.32/SC	1.5(5)	1.904(9)	0.005(1)	1.3*	2.51(1)	0.0079(7)	6.0(7)	2.54(1)	0.0072(7)
NiZn0.5/SC	1.1(5)	1.89(1)	0.009(1)	1.8(6)	2.51(1)	0.0080(7)	5.5(6)	2.55(1)	0.0076(6)

(b)

Sample	N_{Ni-Ni}	R_{Ni-Ni}	σ^2_{Ni-Ni}	N_{Ni-Zn}	R_{Ni-Zn}	σ^2_{Ni-Zn}
Ni foil	12*	2.489(5)	0.0060(6)	–	–	–
Ni/SC	10.4(9)	2.47(1)	0.0060(8)	–	–	0.0060(8)
NiZn0.08/SC	9.5(7)	2.48(1)	0.0060(5)	0.8*	2.51(1)	0.0062(5)
NiZn0.125/SC	9.4(8)	2.48(2)	0.0062(8)	1.0(6)	2.51(1)	0.0066(8)
NiZn0.2/SC	8.1(9)	2.49(2)	0.0064(8)	1.9(7)	2.53(1)	0.0070(8)
NiZn0.32/SC	7.9(8)	2.49(2)	0.0064(7)	2.1(8)	2.54(1)	0.0072(7)
NiZn0.5/SC	5.6(8)	2.49(2)	0.0063(1)	3.0(8)	2.55(1)	0.0076(6)

N average coordination number; R interatomic distance [Å]; σ^2 Debye-Waller factor [Å^2]; * Fixed parameter.

Table 5
Catalytic activity of Ni/SC, Ni/SC functionalized and NiZn/SC.

	X_T (%)	X_L (%)	Selectivity to liquid products (%)						
			MeOH	EtOH	AcO	1-POH	AcOH	EG	1,2-PG
Test (i)									
Ni/SC	37.0	35.5	0.9	3.1	0.2	2.3	3.3	8.5	81.7
Ni/SC80	52.0	49.0	0.3	1.6	0.1	1.1	1.8	10.2	84.9
Ni/SC100	44.0	41.0	1.6	4.8	0.2	0.8	7.9	6.4	78.3
NiZn0.08/SC	50.8	47.8	0.8	1.9	0.3	3.2	4.5	7.7	81.6
NiZn0.125/SC	55.0	51.8	0.6	1.5	0.2	2.7	3.4	6.7	84.9
NiZn0.2/SC	58.6	55.7	0.9	1.2	0.2	2.7	2.7	5.6	86.7
NiZn0.32/SC	60.4	57.5	0.8	1.3	0.2	2.4	3.4	6.1	85.8
NiZn0.5/SC	53.2	50.7	0.6	1.0	0.2	2.5	2.6	6.4	86.7
Test (ii)									
Ni/SC	18	16.5	3.0	1.8	1.6	3.2	73.1	3.3	14.0
Ni/SC80	30	27.5	3.3	0.8	1.4	0.3	84.0	3.5	6.7
NiZn0.20/SC	51	47.0	4.1	1.7	2.4	1.1	66.2	5.8	18.7
Test (iii)									
Ni/SC	80	78.5	0.7	1.2	0.4	0.7	–	0.0	97.0
Ni/SC80	85	82.6	0.9	1.4	0.4	0.5	–	0.0	96.8

Reaction conditions:
Test (i): 30 wt% glycerol aqueous solution, 0.3 g catalyst, 260 °C, p_{H2}^{00} = 2 MPa, 2 h.
Test (ii): 30 wt% glycerol aqueous solution, 0.2 g catalyst, 260 °C, p_{N2}^{00} = 2 MPa, 2 h.
Test (iii): 1 wt% acetol aqueous solution, 0.02 g catalyst, 200 °C, p_{H2}^{00} = 2 MPa, 2 h.

C—O bond cleavage and allows comparing the effect of the support versus the addition of Zn. Table 5 shows that the bimetallic NiZn0.2/SC catalyst is much more active (X_L = 47%) than Ni/SC80 (X_L = 27%), despite the greater acidic strength of the Ni/SC80 catalyst (Fig. 2b). This shows that the addition of Zn, between 0.2 and 0.32 Zn/Ni atomic ratio, allows reaching higher conversions and selectivities towards 1,2 PG, compared with the acidification of the support through the treatment with nitric acid.

4. Conclusions

The aim of this work was to improve the catalytic properties of catalyst Ni/SC by either modifying the support or adding a metallic promoter.

The functionalization of the SC support to 80 °C employing HNO_3 at 60 wt% as oxidizing agent allowed increasing the number of surface acid sites that provide Lewis-type acidity without loss of specific surface area.

The modification of the metallic phase by the addition of Zn applying a controlled preparation technique (SOMC/M) allowed the selective addition of small amounts of Zn on the Ni particles. This was confirmed by the characterization results through EXAFS and XRD which show that all Zn is in interaction with Ni.

The addition of 1–1.8% of Zn (which corresponds to catalysts NiZn0.2/SC and NiZn0.32/SC) generates the formation of an active site composed of an α-NiZn alloy that could be responsible for the increase in activity. When the addition of Zn is higher (2.8 wt%, which corresponds to catalyst NiZn0.5/SC), the generation of a new tetragonal phase of β_1-NiZn could cause the decrease of catalytic activity. These results indicate that the Zn addition has a more significant effect upon the activity and selectivity on the C—O bond cleavage reactions than the effect of the support acidity upon the dehydration activity.

Acknowledgments

The authors thank CONICET (Consejo Nacional de Investigaciones Científicas y Técnicas), PIP 611 and PIP 1035; “Universidad Nacional de La Plata” (UNLP-I-175); ANPCyT - (Agencia Nacional de Promoción Científica y Tecnológica), PICT 2015-2285 and Laboratorio Nacional de Luz Sincrotron (LNLS), Campinas, Brazil (Proposal XAFS2- 20160632). The authors thank Pablo Fetsis for the BET measurements, Lilian Osiglio for the potentiometric titration measurements.

Appendix A. Supplementary data

Supplementary data associated with this article can be found, in the online version, at http://dx.doi.org/10.1016/j.apcata.2017.08.037.

References

[1] D. Sun, Y. Yamada, S. Sato, W. Ueda, Appl. Catal. B: Environ. 193 (2016) 75–92.
[2] S. García-Fernández, I. Gandarias, J. Requies, F. Soulimani, P.L. Arias, B.M. Weckhuysen, Appl. Catal. B: Environ. 204 (2017) 260–272.
[3] M. Balaraju, V. Rekha, P.S. Sai Prasad, B.L.A. Prabhavathi Devi, R.B.N. Prasad, N. Lingaiah, App. Catal. A: Gen. 354 (2009) 82–87.
[4] N. Hamzah, N.M. Nordin, A.H.A. Nadzri, Y.A. Nik, M.B. Kassim, M.A. Yarmo, Appl. Catal. A: Gen. 419–420 (2012) 133–141.
[5] J.B. Salazar, D.D. Falcone, H.N. Pham, A.K. Datye, F.B. Passos, R.J. Davis, Appl. Catal. A: Gen. 482 (2014) 137–144.
[6] B. Mallesham, P. Sudarsanam, B.V.S. Reddy, B.M. Reddy, Appl. Catal. B: Environ. 181 (2016) 47–57.
[7] Y. Li, H. Liu, L. Ma, D. He, Appl. Catal. A: Gen. 522 (2016) 13–20.
[8] E.S. Vasiliadou, E. Heracleous, I.A. Vasalos, A.A. Lemonidou, Appl. Catal. B: Environ. 92 (2009) 90–99.
[9] M. Besson, P. Gallezot, C. Pinel, Chem. Rev. 114 (2014) 1827–1870.
[10] M.A. Dasari, P.P. Kiatsimkul, W.R. Sutterlin, G.J. Suppes, Appl. Catal. A: Gen. 281 (2005) 225–231.
[11] T. Miyazawa, Y. Kusunoki, K. Kunimori, K. Tomishige, J. Catal. 240 (2006) 213–221.
[12] A. Wawrzetz, B. Peng, A. Hrabar, A. Jentys, A.A. Lemonidou, J.A. Lercher, J. Catal. 269 (2010) 411–420.
[13] I. Gandarias, P.L. Arias, J. Requies, M.B. Guemez, J.L.G. Fierro, Appl. Catal. B: Environ. 97 (2010) 248–256.
[14] S. Xia, R. Nie, X. Lu, L. Wang, P. Chen, Z. Hou, J. Catal. 296 (2012) 1–11.
[15] L. Guo, J. Zhou, J. Mao, X. Guo, S. Zhang, Appl. Catal. A: Gen. 367 (2009) 93–98.
[16] J. Zhao, W. Yu, C. Chen, H. Miao, H. Ma, J. Xu, Catal. Lett. 134 (2009) 184–189.
[17] A. Von-Held Soares, G. Perez, F.B. Passos, Appl. Catal. B: Environ. 185 (2016) 77–87.
[18] S.M. Pudi, P. Biswas, S. Kumar, B. Sarkar, J. Braz. Chem. Soc. 26 (8) (2015) 1551–1564.
[19] B. Chen, B. Zhang, Y. Zhang, X. Yang, ChemCatChem 8 (2016) 1929–1936.
[20] M.N. Gatti, F. Pompeo, G.F. Santori, N.N. Nichio, Catal. Today (2017), http://dx.doi.org/10.1016/j.cattod.2017.04.003.
[21] D.V. Cesar, G.F. Santori, F. Pompeo, M.A. Baldanza, C.A. Henriques, E. Lombardo, M. Schmal, L. Cornaglia, N.N. Nichio, Int. J. Hydrogen Energy 41 (2016) 22000–22008.
[22] J.A. Bearden, Rev. Mod. Phys. 39 (1967) 78–124.
[23] B. Ravel, M. Newville, J. Synchrotron Radiat. 12 (2005) 537–541.
[24] S.I. Zabinsky, J.J. Rehr, A. Ankudinov, R.C. Albers, M.J. Eller, Phys. Rev. B 52 (1995) 2995–3009.

[25] R.P. Anantatmula, D.B. Masson, Metall. Trans. 5 (1974) 605–613.
[26] B. Huang, C.H. Bartholomew, B.F. Woodfield, Microporous Mesoporous Mater. 184 (2014) 112–121.
[27] M.N. Gatti, B. Lombardi, D. Gazzoli, G.F. Santori, F. Pompeo, N.N. Nichio, Catalysts 7 (2017) 6.
[28] C. Alegre, M.E. Gálvez, E. Baquedano, E. Pastor, R. Moliner, M.J. Lázaro, Int. J. Hydrogen Energy 37 (2012) 7180–7191.
[29] N. Mager, N. Meyer, A.F. Léonard, N. Job, M. Devillers, S. Hermans, Appl. Catal. B: Environ. 148–149 (2014) 424–435.
[30] H. Ding, J. Li, Y. Gao, D. Zhao, D. Shi, G. Mao, S. Liu, X. Tan, Powder Technol. 284 (2015) 231–236.
[31] T. Niu, G.L. Liu, Y. Liu, Appl. Catal. B: Environ. 154–155 (2014) 82–92.
[32] R. Dong, W. Yang, P. Wu, M. Hussain, Z. Xiu, G. Wu, P. Wang, Mat. Charact. 103 (2015) 37–41.
[33] Z. Omidin, A. Ghasemi, S. Bakhshi, Ceram. Int. 41 (2015) 5779–5784.
[34] B. Lombardi, F. Pompeo, A.N. Scian, N.N. Nichio, Mat. Lett. 106 (2013) 393–395.
[35] Z.Q. Li, C.J. Lu, Z.P. Xia, Y. Zhou, Z. Luo, Carbon 45 (2007) 1686–1695.
[36] R. Cid, G. Pecchi, Appl. Catal. 14 (1985) 15–21.
[37] L. Pizzio, M. Blanco, Microporous Mesoporous Mater. 103 (2007) 40–47.
[38] A. Gervasini, J. Fenyvesi, A. Auroux, Catal. Lett. 43 (1997) 219–228.
[39] G. Zhang, Z. Li, H. Zheng, T. Fu, Y. Ju, Y. Wang, Appl. Catal. B: Environ. 179 (2015) 95–105.
[40] P. Melo, R. Jiménez, A. Karelovic, XXV Iberoamerican Congress on Catalysis (2016).
[41] W.B. Pearson, L.T. Thompson, Can. J. Phys. 35 (1957) 349–357.
[42] M. Friedrich, D. Teschner, A. Knop-Gericke, M. Armbrüster, J. Phys. Chem. C 116 (2012) 14930–14935.
[43] G.P. Vassilev, T. Gomez-Acebo, J.C. Tedenac, J. Phase Equilibria 21 (2000) 287–301.
[44] L.J. Giovanetti, J.M. Ramallo-López, M. Foxe, L.C. Jones, M.M. Koebel, G.A. Somorjai, A.F. Craievich, M.S. Salmeron, F.G. Requejo, Small 8 (3) (2012) 468–473.
[45] S. Xia, R. Nie, X. Lu, L. Wang, P. Chen, Z. Hou, J. Catal. 296 (2012) 1–11.
[46] X. Li, C. Zhang, H. Cheng, L. He, W. Lin, Y. Yu, F. Zhao, J. Mol. Catal. A: Chem. 395 (2014) 1–6.